Preprints.org

Article

Not peer-reviewed version

Highly Efficient Adsorption of Uranium(VI) Ions in Aqueous Solution by Imidazole-4,5-dicarboxylic Acid Functionalized UiO-66

Tian Lan , Xiechun Liu , Haifeng Cong , Xiaofan Ding * , Jing Zhao * , Songtao Xiao *

Posted Date: 28 May 2025

doi: 10.20944/preprints202505.2163.v1

Keywords: metal-organic framework; imidazole - 4,5 - dicarboxylic Acid; UiO-66(Zr); high uranium adsorption capacity; high selectivity

Preprints.org is a free multidisciplinary platform providing preprint service that is dedicated to making early versions of research outputs permanently available and citable. Preprints posted at Preprints.org appear in Web of Science, Crossref, Google Scholar, Scilit, Europe PMC.

Copyright: This open access article is published under a Creative Commons CC BY 4.0 license, which permit the free download, distribution, and reuse, provided that the author and preprint are cited in any reuse.

Preprints.org (www.preprints.org) | NOT PEER-REVIEWED | Posted: 28 May 2025 doi:10.20944/preprints202505.2163.v1

Disclaimer/Publisher's Note: The statements, opinions, and data contained in all publications are solely those of the individual author(s) and contributor(s) and not of MDPI and/or the editor(s). MDPI and/or the editor(s) disclaim responsibility for any injury to people or property resulting from any ideas, methods, instructions, or products referred to in the content.

Article

Highly Efficient Adsorption of Uranium(VI) Ions in Aqueous Solution by Imidazole-4,5-dicarboxylic Acid Functionalized UiO-66

Tian Lan, Xiechun Liu, Haifeng Cong, Xiaofan Ding *, Jing Zhao * and Songtao Xiao *

Department of Radiochemistry, China Institute of Atomic Energy, Beijing 102413, China

* Correspondence: xiaofan_ding@163.com (X.D.); zhaojing.mail@qq.com (J. Z.); xiao_songtao@126.com (S. X.)

Abstract: In this study, a novel adsorbent, UiO-66-H3IMDC, was successfully prepared by functionalizing UiO-66 with imidazole - 4,5 - dicarboxylic Acid (H3IMDC). The effective functionalization of H3IMDC on UiO-66 was confirmed by Powder X-ray Diffraction (PXRD) and Fourier Transform Infrared Spectroscopy (FT-IR). The relationships between the adsorption of U(VI) on UiO-66-H3IMDC and the contact time, the pH of the solution, as well as the initial concentration of U(VI) were investigated. Additionally, the selective adsorption of U(VI) by UiO-66-H3IMDC and its cyclic regeneration performance were also studied. The results demonstrate that the UiO-66-H3IMDC adsorbent exhibits excellent adsorption performance for uranium in aqueous solutions.

Keywords: metal-organic framework; imidazole - 4,5 - dicarboxylic Acid; UiO-66(Zr); high uranium adsorption capacity; high selectivity

1. Introduction

During uranium mining, nuclear fuel processing, nuclear power generation, and spent fuel reprocessing, substantial amounts of uranium-containing radioactive waste are generated [1]. Upon entering the human body, uranium primarily accumulates in the liver, kidneys, and skeletal system, potentially causing acute / chronic poisoning, multi-organ diseases, hepatic damage, and carcinogenic effects. Effective management of such radioactive waste is imperative, with uranium-contaminated wastewater treatment representing a critical component of radwaste disposal [2]. Currently, the treatment methods are divided into three major categories: chemical methods [3], physical-chemical methods [4], and biological methods [5]. Specific treatment technologies include traditional methods such as evaporation concentration [6], chemical precipitation [7], ion exchange [8], electrochemical method [9], and microbial treatment [10]. With the development of materials science, new types of adsorbent materials keep emerging, and the treatment of radioactive wastewater by the adsorption method has received special attention in recent years [11].

Metal-organic frameworks (MOFs) are a class of porous crystalline materials composed of organic ligands connected via coordination bonds [12]. These extensively studied materials demonstrate exceptional potential for radioactive wastewater remediation due to their unique combination of properties, including tunable pore architectures, structural customizability, and high crystallinity. While pristine MOFs typically exhibit limited intrinsic adsorption capacities for radionuclides, targeted modifications have been shown to significantly enhance their adsorption performance. This optimization enables more efficient removal of radioactive species such as uranyl ions (UO_2^{2+}) from contaminated water systems.

Understandably, MOFs serving as adsorbents require stability in aqueous or acidic environments. A breakthrough came with Lillerud and colleagues' synthesis of a zirconium(IV) dicarboxylate porous material, designated as UiO-66 [13]. This framework demonstrated exceptional surface area and unprecedented chemical stability, establishing a new benchmark in the field. Subsequent research efforts have extensively investigated the uranyl ion (UO_2^{2+}) adsorption

© 2025 by the author(s). Distributed under a Creative Commons CC BY license.

Preprints.org (www.preprints.org) | NOT PEER-REVIEWED | Posted: 28 May 2025 doi:10.20944/preprints202505.2163.v1

capabilities of both pristine UiO-66 and its structural analogs, driving innovations in nuclear waste treatment technologies. Luo et al. [14] studied the ability of UIO-66-NH_2 to capture U(VI) from an aqueous solution. Under the condition of pH 5.5, the adsorption of U(VI) reached equilibrium in approximately 4 hours, and the maximum adsorption capacity was 114.9 mg g^{-1}. RAJAEI et al. [15] studied the modification of UIO-66 and vacant UIO-66 (UiO-66-vac) by immobilizing tributyl phosphate (TBP), and these modified materials were used for the removal of uranyl ions from an aqueous solution. The research results showed that the maximum adsorption capacities of UiO-66-TBP, and UiO-66-vac-TBP for uranium were 201.9, and 203.5 mg g^{-1}, respectively. That is, the immobilization of TBP significantly enhanced the adsorption capacity of MOFs for uranyl ions. It can be seen that although researchers have carried out various modifications on UiO-66 to improve its uranium adsorption capacity, the results are not entirely satisfactory. Therefore, on the basis of taking into account the high chemical stability of UiO-66, it is of great significance to explore how to develop a functionalized UiO-66 adsorbent with a high adsorption capacity.

Imidazole-4,5-dicarboxylic acid (H_3IMDC) is a versatile ligand containing imidazole nitrogen and two carboxyl groups [16]. Its molecular structure features two carboxylic acid groups and an imidazole ring nitrogen atom, which together provide multiple coordination sites to form stable chelates with metal ions [17]. Metal complexes derived from this ligand exhibit strong stability under high-temperature and chemically harsh environments, making them advantageous for the regeneration and reuse of adsorbent materials [18]. Furthermore, the amphoteric nature of the imidazole ring - capable of protonation / deprotonation—enables it to maintain adsorption activity across a broad pH range, allowing adaptability to diverse wastewater treatment conditions [19]. This unique combination of structural and chemical properties positions imidazole-4,5-dicarboxylic acid as a promising candidate for designing robust and reusable materials for environmental remediation applications [20–22].

Therefore, in this study, UiO-66(Zr) was functionalized with H_3IMDC to enhance its uranium adsorption performance. Compared to pristine UiO-66 and H_3IMDC individually, the UiO-66-H_3IMDC composite exhibited a significant improvement in U(VI) ion adsorption capacity. Key factors influencing adsorption behavior - including pH, initial U(VI) concentration, contact time, ionic competition, and regeneration cycles - were systematically investigated. Furthermore, Fourier transform infrared (FT-IR) spectroscopy was employed to elucidate the adsorption mechanism of UiO-66-H_3IMDC.

2. Results and Discussion

2.1. Characterization of MOFs

Figure 1a displays the PXRD patterns of UiO-66, UiO-66-H_3IMDC, and pristine H_3IMDC. The characteristic diffraction peaks of both UiO-66 and H_3IMDC are distinctly present in the UiO-66-H_3IMDC composite. This dual observation not only confirms the successful synthesis of crystalline UiO-66-H_3IMDC but also demonstrates the effective functionalization of UiO-66 through H_3IMDC incorporation. Additionally, Figure 1b presents the Fourier transform infrared (FT-IR) spectra of pristine UiO-66, H_3IMDC, and UiO-66-H_3IMDC. The absorption peak at 3174 cm^{-1} corresponds to N-H stretching vibrations inherent in the pure H_3IMDC ligand [20]. Following H_3IMDC modification, significant spectral shifts emerge in two critical regions: both the C-N (1469 - 1457cm^{-1}) and O-C=O (1585 -1578 cm^{-1}, 1389 - 1397 cm^{-1}) characteristic peaks exhibit notable displacement compared to their original positions in pure H_3IMDC. And the O-C=O vibrational signature in UiO-66-H_3IMDC (1397 cm^{-1}, 1578 cm^{-1}) displays marked deviation from its counterpart in pristine UiO-66 (1395 cm^{-1}, 1583 cm^{-1}) [23]. These spectral discrepancies collectively confirm the successful covalent grafting of H_3IMDC onto the UiO-66 framework. The N_2 adsorption-desorption isotherms of UiO-66 and UiO-66-H_3IMDC at 77 K exhibit classical Type I behavior (Figure 1c) , confirming their microporous architectures. Post-functionalization, UiO-66-H_3IMDC demonstrates a substantial reduction in BET surface area (from 1297.5 m^2 g^{-1} to 604.2 m^2 g^{-1}), primarily due to partial pore blockage caused by

© 2025 by the author(s). Distributed under a Creative Commons CC BY license.

Preprints.org (www.preprints.org) | NOT PEER-REVIEWED | Posted: 28 May 2025 doi:10.20944/preprints202505.2163.v1

H_3IMDC grafting. This steric hindrance effect arises from the chelation of H_3IMDC carboxylate groups to $Zr_6O_4(OH)_4$ clusters, which modifies the pore accessibility while preserving the overall framework crystallinity.

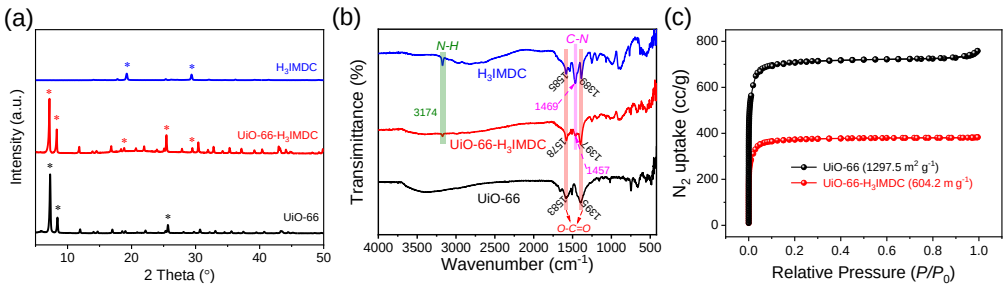

Figure 1. (a) PXRD pattern and (b) infrared spectra of UiO-66, UiO-66-H_3IMDC, and pristine H_3IMDC, (c) N_2 adsorption-desorption isotherm at 77 K of UiO-66 and UiO-66-H_3IMDC.

Furthermore, Figure 2 displays the morphological characteristics of UiO-66 and UiO-66-H_3IMDC, respectively. As can be observed, UiO-66 exhibits a smooth surface morphology. Upon grafting H_3IMDC onto UiO-66, the crystal structure of the parent material remains intact and undamaged. Notably, irregular particles become distinctly visible and dispersed across the surface of UiO-66-H_3IMDC, as highlighted by the circular markers.

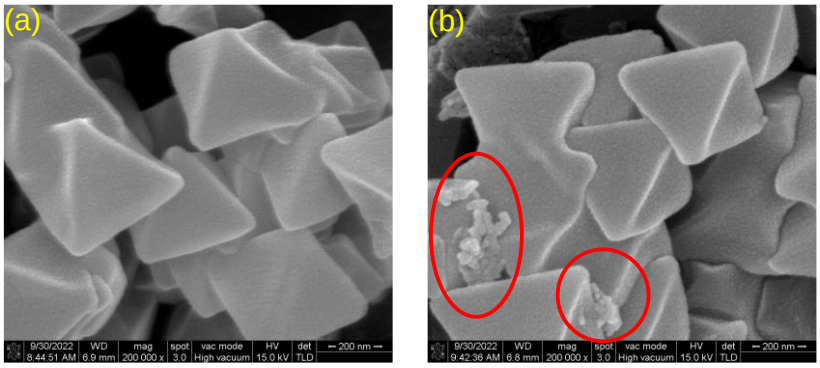

Figure 2. SEM images of (a) UiO-66 and (b) UiO-66-H_3IMDC.

2.2. Effect of initial pH

Given that solution pH significantly influences the protonation and deprotonation of functional groups on the adsorbent surface, as well as the speciation of metal ions in solution [24], we prioritized exploring the impact of pH on our adsorption experiments. Figure 3a illustrates the adsorption outcomes of UiO-66-H_3IMDC for U(VI) at various pH levels. Notably, the adsorption capacity for U(VI) is relatively low at low pH values. This can be attributed to the high concentration of H^+ ions in the solution at low pH, which compete with U(VI) ions for adsorption sites on the UiO-66-H3IMDC surface. As the pH increases, the competitive interaction between U(VI) and H^+ diminishes, and the adsorption capacity reaches its peak at pH = 6. On the other hand, pH-induced U(VI) speciation may also account for the pH-dependent adsorption. It is well-known that as the pH increases, the U(VI) species gradually transform from free UO_2^{2+} to polynuclear hydroxide complexes (Figure 3b). These hydroxide complexes are likely to be more favorably adsorbed by the adsorbent. In the subsequent experiments, a pH of 6.0 was selected as an appropriate condition for further investigation.

© 2025 by the author(s). Distributed under a Creative Commons CC BY license.

Preprints.org (www.preprints.org) | NOT PEER-REVIEWED | Posted: 28 May 2025 doi:10.20944/preprints202505.2163.v1

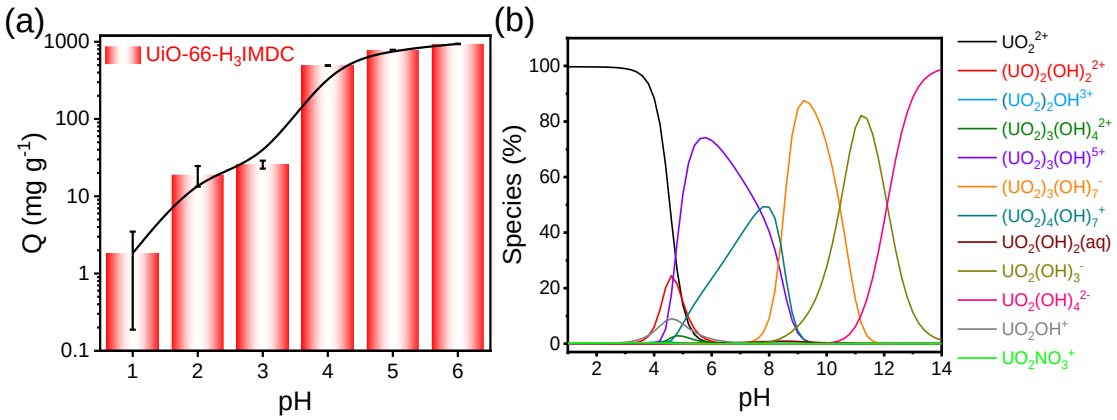

Figure 3. (a) Effect of pH on UiO-66-H3IMDC on U (VI) adsorption (adsorbent dosage=3 mg; C_0=300 mg L^{-1}; t=8 h; T=298.15 K); (b) Variation of Th (IV) species with pH of aqueous solution (Visual Minteq-3.1 program).

2.3. Adsorption Isotherm

The uranium sorption performance of UiO-66, H3IMDC, and UiO-66-H3IMDC was systematically evaluated. As shown in Figure 4a, the adsorption isotherms of these three materials exhibit a significant enhancement in uranium uptake capacity after functionalization. The maximum sorption capacities of UiO-66, H3IMDC, and UiO-66-H3IMDC within the tested concentration range were determined as 235.5, 605.3, and 942.8 mg g^{-1}, respectively. The UiO-66-H3IMDC demonstrates exceptional uranyl ion (UO_2^{2+}) adsorption capacity that significantly surpasses most MOF-based adsorbents reported in current literature (Table S1). Despite the substantially reduced BET surface area of the functionalized UiO-66 (attributed to pore-blocking effects from H3IMDC coordination), the integration of H3IMDC introduced high-efficiency binding sites (e.g., carboxylate and imidazole groups), enabling exceptional uranium affinity that compensates for porosity loss.

To elucidate the sorption mechanism, the adsorption data were fitted with two classical isotherm models, Langmuir and Freundlich models [25,26]:

Langmuir isotherm equation:

$$\frac{C_e}{Q_e} = \frac{1}{K_L Q_m} + \frac{C_e}{Q_m} \quad (2)$$

Freundlich isotherm equation:

$$lnQ_e = lnK_F + \frac{1}{n} lnC_e \quad (3)$$

where C_e (mg L^{-1}) denotes the equilibrium U(VI) concentration in the aqueous phase, Q_e (mg g^{-1}) represents the equilibrium adsorption capacity, and Q_m (mg g^{-1}) corresponds to the theoretical maximum adsorption capacity derived from the Langmuir isotherm model. The parameter K_L is the Langmuir affinity constant, while K_F and n are the Freundlich constants characterizing adsorption capacity and heterogeneity, respectively.

The experimental versus modeled adsorption profiles for the Langmuir and Freundlich isotherms are comparatively visualized in Figure 4b,c, with detailed fitting parameters and correlation coefficients (R^2) tabulated in Table S2. Notably, the Langmuir model demonstrates superior agreement (R^2 = 0.992) over the Freundlich model (R^2 = 0.984). This pronounced preference for the Langmuir isotherm strongly supports a monolayer adsorption mechanism governed by homogeneous active sites across the adsorbent surface, where U(VI) species undergo chemo selective coordination with the imidazole-dicarboxylate functionalities of UiO-66-H3IMDC.

© 2025 by the author(s). Distributed under a Creative Commons CC BY license.

Preprints.org (www.preprints.org) | NOT PEER-REVIEWED | Posted: 28 May 2025 doi:10.20944/preprints202505.2163.v1

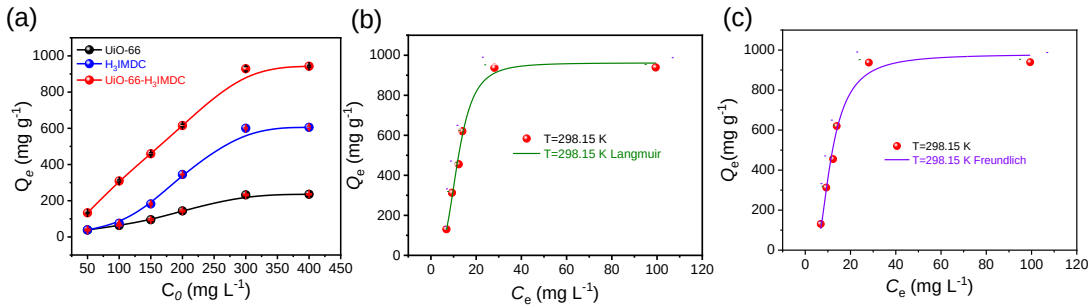

Figure 4. (a) Adsorption isotherms of UiO-66, H_3IMDC, and UiO-66-H_3IMDC (T= 298.15 K, t=8 h; pH=6.0); (b) Langmuir model and (c) Freundlich model of UiO-66-H_3IMDC.

2.4. Adsorption Kinetics

The adsorption kinetics were investigated through time-dependent batch experiments, with the temporal evolution of adsorption capacity quantified in Figure 5a. Kinetic analysis revealed a triphasic adsorption mechanism: (1) an initial rapid adsorption stage (0 - 100 min) dominated by surface complexation, (2) a transitional diffusion-controlled phase (100 - 300 min) showing progressive site saturation, and (3) an equilibrium plateau (> 300 min) achieving maximum adsorption capacity. Notably, > 60% of total uranium uptake occurred within the first kinetic phase, followed by gradual pore-filling processes until complete monolayer formation.

The interfacial mass transfer mechanisms governing U(VI) adsorption on UiO-66-H_3IMDC were elucidated through kinetic modeling using two classical formulations [27,28]: the pseudo-first-order-model (PFO) (Eq. 4) for physisorption-dominated processes and the pseudo-second-order model (PSO) (Eq. 5) describing chemisorption-controlled systems. The linearized rate equations are mathematically expressed as:

$$\ln(Q_e\text{-}Q_t)=\ln Q_e\text{-}k_1 t \quad (4)$$

$$\frac{t}{Q_t}=\frac{1}{k_2 Q_e^2}+\frac{t}{Q_e} \quad (5)$$

where k_1 (min^{-1}) and k_2 (g/mg•min) are the adsorption constants. Q_e and Q_t denote the amount of adsorption (mg/g) at the equilibrium moment and t (min) moment, respectively.

Figure 5b,c present the nonlinear regression analysis of kinetic models, with corresponding goodness-of-fit statistics detailed in Table S3. The pseudo-second-order (PSO) model demonstrates superior predictive capability, evidenced by its coefficient of determination (R^2 = 0.927) significantly exceeding that of the pseudo-first-order (PFO) model (R^2 = 0.796). This high degree of correlation establishes through rigorous statistical validation that the U(VI) adsorption process on UiO-66-H_3IMDC follows PSO kinetics, indicative of rate-limiting chemisorption mechanisms potentially involving surface complexation or ion-exchange reactions.

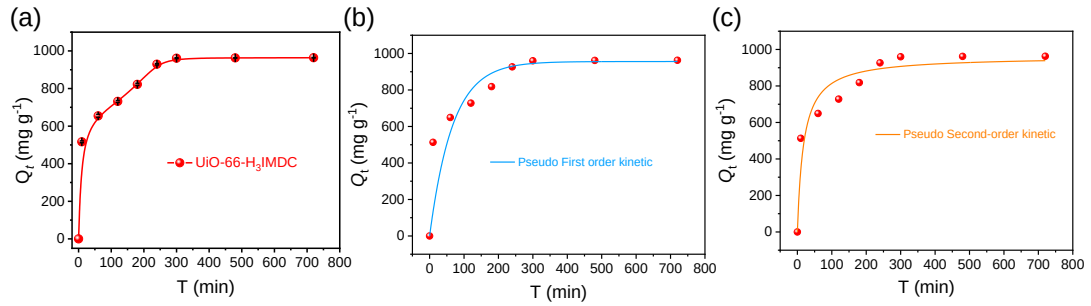

Figure 5. (a) Effect of uranium adsorption time on UiO-66-H_3IMDC (C_0=300 mg L^{-1}; T=298.15 K; pH=6.0); (b) pseudo first-order model and (c) the pseudo second-order model fitting curve.

© 2025 by the author(s). Distributed under a Creative Commons CC BY license.

Preprints.org (www.preprints.org) | NOT PEER-REVIEWED | Posted: 28 May 2025 doi:10.20944/preprints202505.2163.v1

2.5. Effect of Co-Existing Ions

The remediation of U(VI) from radioactive wastewater necessitates adsorbents with exceptional ion-discrimination capability, given the inherent challenges posed by heterogeneous ionic matrices containing competing cations. In this study, we ascertained the selective adsorption capabilities of U(VI) in multi-ionic solutions, and the obtained results are presented in Figure 6. After the adsorption process, the concentration of U(VI) ions in the coexisting solution is markedly lower than that of other coexisting ions. Notably, the presence of interfering ions does not impede the adsorption of U(VI) by UiO-66-H_3IMDC. Thus, this material may be used in treatment of real radioactive wastewater.

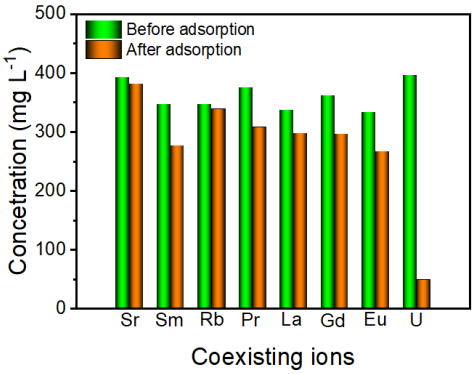

Figure 6. The effect of interfering ions on adsorption capacity for Th (IV) ion onto UiO-66-H_3IMDC. (C^{M+}=300 mg L^{-1}; t=8 h; pH=6.0; T=298.15K).

2.6. Regeneration and Stability Investigation

In practical scenarios, guaranteeing the reusability and stability of adsorbents is essential. As a result, both the adsorption efficiency and the adsorption capacity throughout the adsorption / desorption cycle have emerged as crucial benchmarks for assessing the performance of adsorbents. As illustrated in Figure 7a, following three regeneration cycles, the adsorption quantity witnesses a 16 % reduction. Significantly, the adsorption rates continue to stay elevated throughout this process. Significantly, UiO-66-H_3IMDC maintained structural integrity with indistinguishable PXRD patterns from the pristine material after 7 - day immersion in aqueous media (pH=6) (Figure 7b), providing robust evidence of its exceptional hydrolytic stability under environmentally relevant conditions.

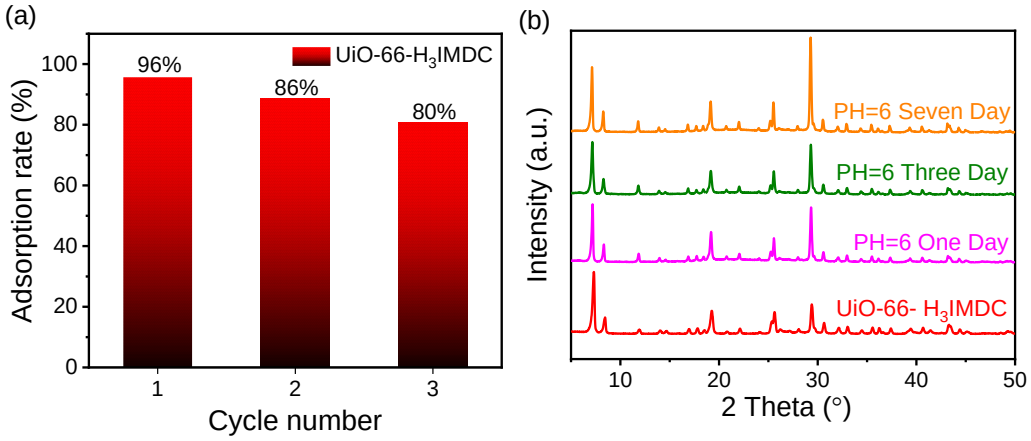

Figure 7. (a) Cyclic regeneration and (b) water stability of UiO-66-H_3IMDC.

© 2025 by the author(s). Distributed under a Creative Commons CC BY license.

Preprints.org (www.preprints.org) | NOT PEER-REVIEWED | Posted: 28 May 2025 doi:10.20944/preprints202505.2163.v1

2.7. Removal Mechanism

Following the adsorption of U(VI), the PXRD patterns of the UiO-66-H_3IMDC show diffraction peaks that precisely match those of the original materials (Figure 8a). This result clearly demonstrates that the crystal structure remains intact during the uranium adsorption process. To further investigate the mechanism of strong chemical interaction between U(VI) ions and UiO-66-H_3IMDC, we compared the infrared (IR) spectral shifts of UiO-66 and UiO-66-H_3IMDC before and after uranium adsorption (Figure 8b,c). Post-adsorption, new O=U=O vibrational bands appeared at 922 cm^{-1} and 911 cm^{-1} [29], directly confirming successful uranium coordination on the material's surface. Notably, the O=U=O peak associated with H_3IMDC exhibited a lower vibrational frequency compared to UiO-66, suggesting a stronger adsorption of U(VI) by H_3IMDC. Additionally, the -COO-Zr doublet peaks in UiO-66-H_3IMDC (1582 - 1577 cm^{-1}, 1405 - 1392 cm^{-1}) underwent significantly larger shifts than those in UiO-66 (1583-1580 cm^{-1}, 1395-1398 cm^{-1}), further evidencing enhanced chemical interactions between UiO-66-H_3IMDC and U(VI), consistent with its superior adsorption capacity. Furthermore, significant shifts in the N-H (3173 - 3718 cm^{-1}) and C-N (1457 - 1469 cm^{-1}) regions indicate that the nitrogen adsorption sites on UiO-66-H_3IMDC also interact with U(VI) ions. The mechanism may be as follows: Firstly, the large specific surface area and abundant porous structure of the UiO-66-H_3IMDC material enable U(VI) species to efficiently diffuse and come into full contact with the composite material. Subsequently, uranyl ions coordinate with the nitrogen- and oxygen-containing active adsorption sites. Therefore, uranium(VI) can not only interact with the surface of the adsorbent but also undergo complexation with more reactive sites.

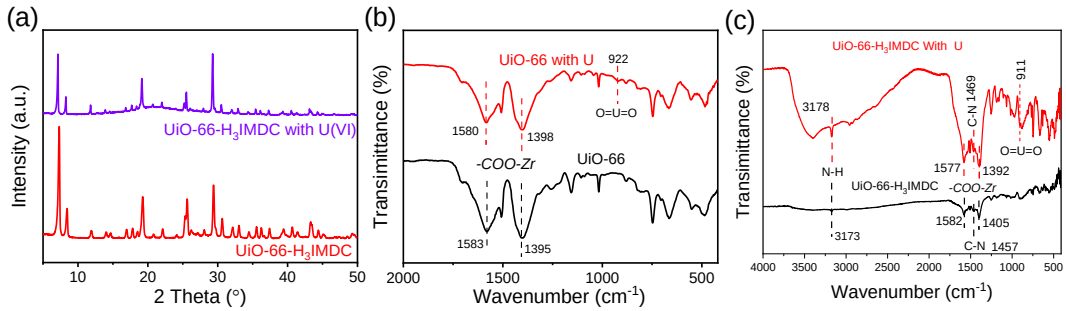

Figure 8. (a) PXRD of UiO-66-H_3IMDC before and after uranium adsorption. FT-IR spectra of (b) UiO-66 and (c) UiO-66-H_3IMDC before and after uranium adsorption.

3. Materials and Methods

3.1. Materials

Zirconyl chloride octahydrate ($ZrOCl_2 \bullet 8H_2O$, AR), terephthalic acid (H_2BDC, >99.0%), 4,5-Imidazoledicarboxylic acid ($C_5H_4N_2O_4$, AR), Acetate ($C_2H_4O_2$, AR), N, N-Dimethylformamide (DMF, >99.5%), and methanol (CH_3OH, AR) were purchased from MACKLIN reagent. Strontium nitrate (SrN_2O_6, AR), cesium nitrate ($CsNO_3$, AR), samarium nitrate hexahydrate ($SmN_3O_9 \cdot 6H_2O$, AR), rubidium nitrate ($RbNO_3$, AR), praseodymium nitrate hexahydrate ($PrN_3O_9 \cdot 6H_2O$, AR), lanthanum nitrate hexahydrate ($LaN_3O_9 \cdot 6H_2O$, AR), gadolinium nitrate hexahydrate ($GdN_3O_9 \cdot 6H_2O$, AR) and europium nitrate hexahydrate ($EuN_3O_9 \cdot 6H_2O$, AR), were purchased from Aladdin (Shanghai, China). uranyl nitrate hexahydrate ($UO_2(NO_3)_2 \cdot 6H_2O$, AR) was obtained from the China Institute of Atomic Energy. Ultrapure water was prepared from the Millipore system (18.25 MΩ•cm) (Direct 8, Millipore, USA). All the above reagents were used directly without further purification.

3.2. Preparation of UiO-66(Zr)

UiO-66(Zr) was synthesized by a solvothermal synthesis technique reported in the literature [31]. H_2BDC (1.6 g) and $ZrOCl_2 \bullet 8H_2O$ (3.2 g) were dissolved in DMF (50 mL) / acetate (50 ml) and

© 2025 by the author(s). Distributed under a Creative Commons CC BY license.

Preprints.org (www.preprints.org) | NOT PEER-REVIEWED | Posted: 28 May 2025 doi:10.20944/preprints202505.2163.v1

mixed completely, then transferred to a 250 mL round-bottomed flask, and stirred at 378.15 K for 24 h under reflux in an oil bath. After that, white powder was obtained through centrifugation. Finally, the sample was washed three times with DMF and three times with methanol, and then dried in a vacuum drying oven to obtain the sample.

3.3. Preparation of UiO-66-H₃IMDC

UiO-66 (Zr) (0.5 g) and H₃IMDC (1.0 g) were dissolved in a solvent mixture of 100 ml ethanol and 50 ml DMF. The mixture was sonicated for 20 minutes to ensure uniform dispersion. After sonication, the solution was subjected to reflux heating at 353.15 K for 24 hours. Upon cooling to room temperature, the product was separated via centrifugation, followed by washing the solid product three times with deionized water and ethanol, respectively. Finally, the material was vacuum-dried overnight to yield the functionalized UiO-66-H₃IMDC composite.

3.4. Characterization Techniques

Powder X-ray diffraction (PXRD) analysis was conducted on a Bruker D8 QUEST diffractometer (Germany) to evaluate the crystallinity and phase purity of the MOF materials. Measurements utilized Cu Kα radiation (λ = 1.542 Å) operated at 40 kV and 40 mA, with a scan range of 4° - 50.0° (2θ) at a rate of 10° min^{-1}.For porosity characterization, nitrogen adsorption-desorption isotherms were recorded at 77 K using a Micromeritics ASAP 2460 analyzer (USA). Prior to analysis, MOF samples (~100 mg) were degassed under vacuum at 80°C for 12 hours to remove physisorbed species. Specific surface areas were calculated via the Brunauer-Emmett-Teller (BET) method. Chemical bonding analysis was performed by Fourier-transform infrared spectroscopy (FT-IR) on a Bruker TENSOR27 spectrometer (Germany). Spectra were acquired in the 400 - 4000 cm^{-1} range to monitor functional group transformations in MOFs. The morphology of the materials were observed using a scanning electron microscope (SEM) (JEM 2100, JEOL, Japan) operating at 30.0 kV under high vacuum conditions. The sample was vacuum-dried and affixed to the test bench with a conductive adhesive before gold sputtering for 80 seconds to facilitate microscopic observation.

3.5. Adsorption Experiments

Batch adsorption experiments were performed by adding 3 mg of adsorbent to 10 mL of U(VI) solution in 15 mL polypropylene centrifuge tubes. The suspensions were agitated at 220 rpm in a temperature-controlled orbital shaker for predetermined time intervals. Subsequently, the mixtures were filtered through 0.22 μm pore-size nylon membranes using a syringe filtration assembly (5 mL capacity). The collected filtrates were acidified with 2% (v/v) HNO_3 and analyzed for residual U(VI) concentrations via inductively coupled plasma optical emission spectrometry (ICP-OES, JY2000-2). Specific experimental parameters (pH, initial U(VI) concentration, and contact time, etc.) are provided in the captions of relevant figures.

The adsorption capacity (Q) of U(VI) was defined by the following equation:

$$Q = \frac{(C_0 - C_e) \times V}{m} \quad (1)$$

where C_0 (mg L^{-1}) and C_e (mg L^{-1}) are the initial concentration and equilibrium concentration of U(VI) ion, respectively. V (L) is the volume of solution, and m (g) is the usage amount of adsorbent.

4. Conclusions

In conclusion, a novel MOF (UiO-66-H₃IMDC) was successfully synthesized through grafting H₃IMDC onto UiO-66, demonstrating exceptional U(VI) adsorption capabilities. The modified material exhibited a maximum U(VI) adsorption capacity of 942.8 mg g^{-1} under optimized conditions (pH = 6), reaching adsorption equilibrium within 300 minutes. Additionally, the uranium adsorption process of UiO-66-H₃IMDC fits better with the Langmuir model and the pseudo-second-order model, indicating that the adsorption process is predominantly a monolayer chemisorption process. Finally,

© 2025 by the author(s). Distributed under a Creative Commons CC BY license.

Preprints.org (www.preprints.org) | NOT PEER-REVIEWED | Posted: 28 May 2025 doi:10.20944/preprints202505.2163.v1

the excellent selectivity and cyclic adsorption ability demonstrated by UiO-66-H_3IMDC suggest that UiO-66-H_3IMDC has the potential to adsorb U(VI) from actual wastewater.

Supplementary Materials: The following supporting information can be downloaded at the website of this paper posted on Preprints.org. Table S1 Langmuir and Freundlich model fitting parameters for U (VI) adsorption. Table S2 Kinetic fitting parameters of U (VI) adsorption in UiO-66-H_3IMDC.

Funding: This research was supported by the Qisun Ye Fund (No. U2441290) and China Institute of Atomic Energy Dean's Fund (No. YZ222505001103).

Institutional Review Board Statement: Not applicable.

Informed Consent Statement: Not applicable.

Data Availability Statement: Dataset available on request from the authors.

Conflicts of Interest: The authors declare no conflicts of interest.

References

1. L. Rodríguez-Penalonga, B.Y. Moratilla Soria, A Review of the Nuclear Fuel Cycle Strategies and the Spent Nuclear Fuel Management Technologies, Energies, **2017**, 10, 1235.
2. R. Zhang, L. Xu, F. Yu, S. Xiao, C. Wang, D. Yuan, Y. Liu, Sulfonated heteroatom co-doped carbon materials with a porous structure boosting electrosorption capacity for uranium (VI) removal, J. Solid State Chem., **2023**, 327, 124262.
3. D. Kadadou, E.A. Said, R. Ajaj, S.W. Hasan, Research advances in nuclear wastewater treatment using conventional and hybrid technologies: Towards sustainable wastewater reuse and recovery, Journal of Water Process Engineering, **2023**, 52, 103604.
4. A. Srivastava, V.K. Parida, A. Majumder, B. Gupta, A.K. Gupta, Treatment of saline wastewater using physicochemical, biological, and hybrid processes: Insights into inhibition mechanisms, treatment efficiencies and performance enhancement, J. Environ. Chem. Eng., **2021**, 9, 105775.
5. Z. Qu, W. Wang, Y. He, Prediction of Uranium Adsorption Capacity in Radioactive Wastewater Treatment with Biochar, Toxics, **2024**, 12, 118.
6. Y. Wang, L. Zhan, H. Chen, J. Mao, H. Chen, X. Ma, L. Yang, Study on the evaporation performance of concentrated desulfurization wastewater and its products analysis, Journal of Water Process Engineering, **2024**, 58, 104862.
7. J. Kang, W. Sun, Y. Hu, Z. Gao, R. Liu, Q. Zhang, H. Liu, X. Meng, The utilization of waste by-products for removing silicate from mineral processing wastewater via chemical precipitation, Water Research, **2017**, 125, 318-324.
8. L. Bernardo José, G. Cordeiro Silva, A. Cláudia Queiroz Ladeira, Pre-concentration and partial fractionation of rare earth elements by ion exchange, Miner. Eng., **2024**, 205, 108477.
9. T. Lin, T. Chen, C. Jiao, H. Zhang, K. Hou, H. Jin, Y. Liu, W. Zhu, R. He, Ion pair sites for efficient electrochemical extraction of uranium in real nuclear wastewater, Nat. Commun., **2024**, 15, 4149.
10. A. Moghaddam, D. Khayatan, P. Esmaeili Fard Barzegar, R. Ranjbar, M. Yazdanian, E. Tahmasebi, M. Alam, K. Abbasi, H. Esmaeili Gouvarchin Ghaleh, H. Tebyaniyan, Biodegradation of pharmaceutical compounds in industrial wastewater using biological treatment: a comprehensive overview, Int. J. Environ. Sci. Technol., **2023**, 20, 5659-5696.
11. D. Mei, L. Liu, B. Yan, Adsorption of uranium (VI) by metal-organic frameworks and covalent-organic frameworks from water, Coord. Chem. Rev., **2023**, 475, 214917.
12. H. Furukawa, K.E. Cordova, M. O'Keeffe, O.M. Yaghi, The Chemistry and Applications of Metal-Organic Frameworks, Science, **2013**, 341, 1230444.
13. J.H. Cavka, S. Jakobsen, U. Olsbye, N. Guillou, C. Lamberti, S. Bordiga, K.P. Lillerud, A New Zirconium Inorganic Building Brick Forming Metal Organic Frameworks with Exceptional Stability, J. Am. Chem. Soc., **2008**, 130, 13850-13851.
14. B.-C. Luo, L.-Y. Yuan, Z.-F. Chai, W.-Q. Shi, Q. Tang, U(VI) capture from aqueous solution by highly porous

© 2025 by the author(s). Distributed under a Creative Commons CC BY license.

Preprints.org (www.preprints.org) | NOT PEER-REVIEWED | Posted: 28 May 2025 doi:10.20944/preprints202505.2163.v1

and stable MOFs: UiO-66 and its amine derivative, J. Radioanal. Nucl. Chem., **2016**, 307, 269-276.

15. A. Rajaei, K. Ghani, M. Jafari, Modification of UiO-66 for removal of uranyl ion from aqueous solution by immobilization of tributyl phosphate, J. Chem. Sci., **2021**, 133, 14.
16. Q.-G. Zhai, R.-R. Zeng, S.-N. Li, Y.-C. Jiang, M.-C. Hu, Alkyl substituents introduced into novel d10-metalimidazole-4,5-dicarboxylate frameworks: synthesis, structure diversities and photoluminescence properties, CrystEngComm, **2013**, 15, 965-976.
17. Y. Zhang, X. Luo, Z. Yang, G. Li, Metal–organic frameworks constructed from imidazole dicarboxylates bearing aromatic substituents at the 2-position, CrystEngComm, **2012**, 14, 7382-7397.
18. J. Chen, B. Liu, Construction of cobalt-imidazole-based dicarboxylate complexes with topological diversity: From metal–organic square to one-dimensional coordination polymer, Inorg. Chem. Commun., **2012**, 22, 170-173.
19. L. Shi, K. Bao, J. Cao, Y. Qian, Sunlight-assisted fabrication of a hierarchical ZnO nanorod array structure, CrystEngComm, **2009**, 11, 2009-2014.
20. Z. Bai, Q. Liu, H. Zhang, J. Liu, J. Yu, J. Wang, High efficiency biosorption of Uranium (VI) ions from solution by using hemp fibers functionalized with imidazole-4,5-dicarboxylic, J. Mol. Liq., **2020**, 297, 111739.
21. J. Li, C. Dai, Y. Cao, X. Sun, G. Li, Q. Huo, Y. Liu, Lewis basic site (LBS)-functionalized zeolite-like supramolecular assemblies (ZSAs) with high CO_2 uptake performance and highly selective CO2/CH4 separation, J. Mater. Chem., **2017**, 5, 21429-21434.
22. D. Banerjee, B.C. Mondal, D. Das, A.K. Das, Use of Imidazole 4,5-Dicarboxylic Acid Resin in Vanadium Speciation, Microchim. Acta, **2003**, 141, 107-113.
23. X. Ding, S. Xiao, T. Wang, Z. Zeng, X. Zhao, Q. Yang, Stability of metal-organic frameworks towards β-ray irradiation: Role of organic groups, Microporous Mesoporous Mater., **2023**, 354, 112533.
24. H. Lei, N. Pan, X. Wang, H. Zou, Facile Synthesis of Phytic Acid Impregnated Polyaniline for Enhanced U(VI) Adsorption, J. Chem. Eng. Data, **2018**, 63, 3989-3997.
25. A. Sayari, S. Hamoudi, Y. Yang, Applications of Pore-Expanded Mesoporous Silica. 1. Removal of Heavy Metal Cations and Organic Pollutants from Wastewater, Chem. Mater., **2005**, 17, 212-216.
26. X. Ding, Z. Zhang, X. Li, K. Ma, T. Jin, Z. Feng, T. Lan, J. Zhao, S. Xiao, Highly radiation-resistant Al-MOF selected based on the radiation stability rules of metal–organic frameworks with ultra-high thorium ion adsorption capacity, Environ. Sci.:Nano, **2024**, 11, 2103-2111.
27. L. Chen, Z. Zhang, S. Xiao, X. Li, S. Zhao, Y. Zhao, C. Yu, Z. Feng, K. Ma, X. Liu, X. Ding, J. Zhao, J. Liu, Efficient capture of thorium ions by the hydroxyl-functionalized sp2c-COF through nitrogen-oxygen cooperative mechanism, Green Chem. Eng., **2024**.
28. X. Li, Z. Zhang, Y. Zhao, L. Chen, C. Yu, X. Liu, S. Zhao, Z. Feng, K. Ma, X. Ding, J. Zhao, S. Xiao, Efficient and rapid adsorption of thorium by sp2c-COF with one-dimensional regular micropores channels, J. Environ. Chem. Eng., **2024**,12, 114066.
29. S. Su, R. Che, Q. Liu, J. Liu, H. Zhang, R. Li, X. Jing, J. Wang, Zeolitic Imidazolate Framework-67: A promising candidate for recovery of uranium (VI) from seawater, Colloids Surf., A, **2018**, 547, 73-80.
30. J.H. Cavka, S. Jakobsen, U. Olsbye, N. Guillou, C. Lamberti, S. Bordiga, K.P. Lillerud, A New Zirconium Inorganic Building Brick Forming Metal Organic Frameworks with Exceptional Stability, J. Am. Chem. Soc., **2008**, 130, 13850-13851.

Disclaimer/Publisher's Note: The statements, opinions and data contained in all publications are solely those of the individual author(s) and contributor(s) and not of MDPI and/or the editor(s). MDPI and/or the editor(s) disclaim responsibility for any injury to people or property resulting from any ideas, methods, instructions or products referred to in the content.

© 2025 by the author(s). Distributed under a Creative Commons CC BY license.